Cork Open Research Archive
Cartlann Taighde Oscailte Chorcaí

Title	A miniaturised autonomous sensor based on nanowire materials platform: the SiNAPS mote
Author(s)	Koshro Pour, Naser; Kayal, M.; Jia, G.; Eisenhawer, B.; Falk, F.; Nightingale, Adrian M.; DeMello, John C.; Georgiev, Yordan M.; Petkov, Nikolay; Holmes, Justin D.; Nolan, Michael; Fagas, Gíorgos
Publication date	2013-05-17
Original citation	KOSHRO POUR, N., KAYAL, M., JIA, G., EISENHAWER, B., FALK, F., NIGHTINGALE, A., DEMELLO, J. C., GEORGIEV, Y. M., PETKOV, N., HOLMES, J. D., NOLAN, M. & FAGAS, G. (2013) A miniaturised autonomous sensor based on nanowire materials platform: the SiNAPS mote. Proceedings of SPIE 8763, Smart Sensors, Actuators, and MEMS VI, Grenoble, France, 24 April. doi:10.1117/12.2017520
Type of publication	Conference item
Link to publisher's version	http://spie.org/ http://dx.doi.org/10.1117/12.2017520 Access to the full text of the published version may require a subscription.
Rights	**© Copyright 2013 Society of Photo-Optical Instrumentation Engineers. One print or electronic copy may be made for personal use only. Systematic reproduction and distribution, duplication of any material in this paper for a fee or for commercial purposes, or modification of the content of the paper are prohibited. http://dx.doi.org/10.1117/12.2017520**
Item downloaded from	http://hdl.handle.net/10468/2467

University College Cork, Ireland
Coláiste na hOllscoile Corcaigh

A miniaturised autonomous sensor based on nanowire materials platform: the SiNAPS mote

Naser Khosro Pour[a], Maher Kayal[a], Guobin Jia[b], Bjoern Eisenhawer[b], Fritz Falk[b], Adrian Nightingale[c], John C. DeMello[c], Yordan M. Georgiev[d], Nikolay Petkov[d], Justin D. Holmes[d], Michael Nolan[d] and Giorgos Fagas[*d]

[a] Ecole Polytechnique Federal Lausanne, Lausanne, Switzerland; [b] Institute of Photonic Technology, Jena, Germany; [c] Imperial College London, London, United Kingdom; [d] Tyndall National Institute, University College Cork, Lee Maltings, Dyke Parade, Cork, Ireland

ABSTRACT

A micro-power energy harvesting system based on core(crystalline Si)-shell(amorphous Si) nanowire solar cells together with a nanowire-modified CMOS sensing platform have been developed to be used in a dust-sized autonomous chemical sensor node. The mote (SiNAPS) is augmented by low-power electronics for power management and sensor interfacing, on a chip area of $0.25mm^2$. Direct charging of the target battery (e.g., NiMH microbattery) is achieved with end-to-end efficiencies up to 90% at AM1.5 illumination and 80% under 100 times reduced intensity. This requires matching the voltages of the photovoltaic module and the battery circumventing maximum power point tracking. Single solar cells show efficiencies up to 10% under AM1.5 illumination and open circuit voltages, V_{oc}, of 450-500mV. To match the battery's voltage the miniaturised solar cells ($\sim 1mm^2$ area) are connected in series via wire bonding. The chemical sensor platform (mm^2 area) is set up to detect hydrogen gas concentration in the low ppm range and over a broad temperature range using a low power sensing interface circuit. Using Telran TZ1053 radio to send one sample measurement of both temperature and H_2 concentration every 15 seconds, the average and active power consumption for the SiNAPS mote are less than 350nW and 2.1 µW respectively. Low-power miniaturised chemical sensors of liquid analytes through microfluidic delivery to silicon nanowires are also presented. These components demonstrate the potential of further miniaturization and application of sensor nodes beyond the typical physical sensors, and are enabled by the nanowire materials platform.

Keywords: Mote, Solar Cells, Silicon Nanowires, Chemical Sensors, Microfluidics, Energy Harvesting, Electronics Design, Low Power

1. INTRODUCTION

1.1 General

The continuous development of portable devices in terms of complexity and functionality, in ever decreasing volumes is inciting a new technological revolution. The basis of this is the advance of ambient intelligence, where electronics seamlessly integrated with any type of environment, will monitor and respond to the user's specifications. Applications can be found in healthcare (e.g., point-of-care diagnostics, e-Health, m-Health), pollution monitoring, building automation, logistics, supply-chain controls and chemical warfare. To enable this vision miniaturized devices are required that communicate wirelessly and are self powered. This capability removes the burden of battery replacement and reduces installation and maintenance costs. There is already an increasing demand for energy-efficient wireless sensor networks (WSN) in different sensing and monitoring applications. Many autonomous WSN solutions have been deployed in various areas, including health and lifestyle, automotive, smart buildings, predictive maintenance (e.g., of machines and infrastructure), and active RFID tags [1-3].

The WSN platforms face the main technological challenges of miniaturization, autonomy and manufacturing cost [4]. Miniaturized primary batteries cannot provide long lifetime and small form factor requirements for these applications. Energy harvesting and charging miniaturized rechargeable batteries are most promising solutions for realizing autonomous WSNs. This implies that the emerging autonomous sensors have to maintain ultra-low power (ULP) duty

---

[*] georgios.fagas@tyndall.ie , www.tyndall.ie

cycles and incorporate an energy harvesting source, an energy storage device and electronic circuits for power management, sensing and communication into a miniaturized system. Also, their use for environmental, security and health monitoring, calls for a paradigm shift which goes beyond the typical monitoring of physical conditions such as light, humidity and temperature. There is a need to develop chemical sensing for a variety of (bio-)molecules whose size, reactivity and signature are varying.

Bearing the above challenging constraints in mind the authors have been working together within the Framework 7 funded SiNAPS project [5] to develop leading edge components that are being incorporated into a single mote. The SiNAPS mote is based on the use of materials nanostructured with a high aspect ratio, that is, nanowires. This nanowire materials platform enables us to: (i) reduce the volume of individual active devices while following low-cost processing and device integration strategies compatible with complementary metal-oxide-semiconductor (CMOS) processes, and (ii) demonstrate (bio-)chemical sensing while keeping the power consumption within the available energy budget. A preliminary account of the integration work was presented at the SPIE Microtechnologies 2013. In this paper, we discuss in more detail our results on optimizing the various components of the SiNAPS mote including the nanowire-based energy harvesting system, the power management unit (PMU) and the microfluidics bio-sensing platform. The sensor interface unit (SIU) is optimized for hydrogen gas sensing in the low ppm range and over a broad temperature range [6].

1.2 Background to the nanowire-enabled SiNAPS mote

Solar cells are the most widely deployed energy harvesting sources that convert incoming photons into electricity. Solar energy is the most abundant and practical form of ambient energy and miniaturized solar cells are already available in the custom sizes as small as $1mm^2$ [7]. Especially for outdoor applications, they are an obvious energy source for autonomous systems, as the source power can reach to $100mW/cm^2$. For Indoor applications, illumination levels are much lower in the order of $100\mu W/cm^2$. Nevertheless, thanks to their high efficiencies, solar cells can be good energy sources for miniaturized autonomous wireless sensor nodes, even in the order of a few cubic millimeters size. There are three generations of solar cells. Today's major PV technology is based on bulk silicon (generation I) with a market share close to 90%. Generation II uses thin film technology and is currently being developed. It does produce solar cells at lower cost in €/W, but to date they also have lower module efficiency, typically about 7% for a-Si and up to about 12% (CdTe, CIGS, Si-tandem). Much effort is now focused on new, potentially lower cost solutions based on nanotechnology [8,9]. Nanocrystals, nanorods, nanowires are envisaged to act either as absorbers or charge conduits or both. Apart from more cost effective processing methods, nanostructures offer a number of advantages over bulk materials or thin films. The device thickness can be scaled down by at least an order of magnitude towards the micrometre scale and below. Also, the band gap is tuneable by changing the size, shape and surface functionalisation of the nanostructure, while charge carrier separation can also be more efficient. The required solar cell area depends on the power needed by the sensor device but the volume and the weight of the device can be rather low if it can be made rather thin. For this purpose, within the SiNAPS mote a solar minimodule was developed based on silicon nanowire solar cells. The nanowires act as a light trapping structure to increase the light absorption in the solar cell, and at the same time they are the photovoltaically active material. Efficiencies competitive within generation II PV technologies have been obtained from materials based on the radial core/shell nanoarchitecture of Si nanowires (SiNWs) [9-13].

Once we have an energy harvesting device, there remains the important question of using this energy source efficiently. At present, complex wireless sensor platforms such as iMote [14] have been realized as printed circuit boards (PCB) and cannot be used for realizing millimeter-scale sensors [3]. Bulky batteries are needed to provide the required peak and average power during sensing and data transmission. In addition, most of standard wireless transmission protocols such as Zigbee transceivers [15] require centimeter-scale antennas. In order to replace the bulky batteries that are generally used in ULP sensors, miniaturized energy storage options such as thin film Li-ion batteries and robust low-power circuits should be developed for sensing and wireless data communication. By using smaller batteries for these low power circuits and developing new wireless transmission methods that require smaller antennas, millimeter-scale wireless sensor will become feasible. However, reducing the size of the sensor reduces not only the cost but also the harvested energy. Reducing the size of the mote reduces also the harvested energy; miniaturized energy harvesters can supply only a few microwatts. In order to meet stringent power requirements of these sensors, the total power consumption of the WSN platform should be minimized by proper circuit design of all power-hungry components, including the wireless transceiver and the sensor interface circuit. For an autonomous energy harvesting system, appropriate energy harvesting sources and energy storage devices should be selected, and the energy harvester circuit must be designed to transfer energy from energy source to energy storage with high efficiency. Different architectures have been used for this purpose

such as inductor-based DC-DC converters [16] and switched capacitor DC-DC converters [17]. The PV characteristics, such as open circuit voltage, short circuit current and maximum power point of the PV module also affect the overall efficiency. Due to the small target size that is in the order of mm^3, the harvested energy is in the order of a few hundred microwatts. This limited power budget affects the system level solution. Theoretically, inductor-based DC-DC converters have the highest efficiency as MPP (Maximum Power Point) tracking techniques can be employed to further increase the efficiency of energy transfer from the PV cell to battery. However, the power consumption of these circuits is normally at least on the order of few hundred microwatts which is the total power budget of the SiNAPS mote. Therefore, a direct charging scheme is implemented using a PV mini-module that provides the matched voltage to the battery and leads to the highest overall efficiency.

For miniaturised biosensors Si nanowires boast excellent electrical and mechanical properties which, combined with their high surface area to volume ratio, make them attractive candidates for applications such as field effect transistors (FETs) [18,19] and sensing devices [20,21]. Research into the use of SiNWs as FET-type sensors began by using chemically grown NWs [20]. Such NWs produced by "bottom-up" methods can be fabricated in large quantities but their incorporation into devices requires precise positioning, alignment and contacting of the nanowire, meaning that device integration is non-trivial. A simpler approach is to produce the NWs in-situ using "top-down" fabrication. This approach also allows increased control over NW length, width, thickness, number, and orientation along the different crystallographic axes of Si - parameters which have been shown to be particularly important for sensing applications [22-25]. To this end, a CMOS-compatible top-down fabrication of nanowire devices to be used in miniaturised sensor modules has been developed. For the bio-chemical sensing, microfluidic channels have long been recognised as ideal tools for manipulation of liquid samples for analysis. A large range of sensing modalities (e.g. electrical, optical) can be integrated with the microchannels and the small channel dimensions mean that a tiny quantity of analyte is required [26]. As such they are an excellent candidate system with which to controllably deliver liquid analyte to electrical sensor devices. Our challenge has been to develop miniaturised microfluidic delivery systems based on polydimethylsiloxane (PDMS) and explore an improved surface functionalisation protocol to render the PDMS hydrophilic so that it enables passive fluid delivery via capillary action. This offers possibility of low-power miniaturised chemical sensors of liquid analytes without need for external pumping or inlets.

2. SYSTEM ARCHITECTURE AND EXPERIMENTAL METHODS

As the harvested energy is intermittent and cannot provide a constant and stable voltage that is needed for reliable operation of electrical circuits it needs to be stored in a rechargeable battery and/or supercapacitor. The storage device should have enough capacity to provide energy for a few hours' operation of the sensor, even without energy harvesting. In addition to capacity, other characteristics, such as size, peak discharge current, nominal operating voltage, cycle life and leakage, affect the autonomous operation of the sensor. In the SiNAPS mote we use the Varta V6HR microbattery, which has a nominal voltage of 1.2 V and can provide a peak discharge current of 18 mA that is much higher than the current required during data transmission. This battery has a large nominal capacity of 6.2 mAh, while its diameter and height are 6.8 mm and 2.15 mm, respectively [27].

In micro-power wireless sensing applications, apart from average power consumption of the wireless transceiver, which is mainly minimized by duty cycling its operation, peak and standby power consumption are also very important. Low peak power ensures that miniaturized batteries with limited peak discharge currents can be used and ultra-low standby power guarantees that the average power consumption can be minimized by heavily duty cycling of data transmission. Although most of the wireless transceivers work with at least 1.8 V supply voltage, there are ultra-low power wireless transceivers with sub-1.2 V voltage, such as TZ1053 [28] or ZL70250 [29]. These sub-1 GHz transceivers have some disadvantages, such as larger size of antennas and lower data rates. However, they are more suited for our application thanks to their much lower peak-power and standby power, compared to state-of-the-art 2.4 GHz transceivers [30].

In the target sensor, all electronic circuits, including the external wireless transceiver, can work with a sub-1.2 V supply voltage, so that additional step-down or step-up circuits are not required. Under typical illumination levels in sensor application where the harvested power is less than a few micro-watts, high efficiency comes from direct charging [31]. The block diagram of the SiNAPS electronics circuit, including the required external components and the main blocks of the solar energy harvester, is shown in Figure 1. Four ~1mm^2 nanowire solar cells are connected in series for the PV energy harvester. The power management unit charges the microbattery with very high efficiency and detects end-of-charge (V_{EOC}) and end-of-discharge (V_{EOD}) voltage levels of the battery disconnecting it from the sensor after reaching V_{EOC} and V_{EOD} limits to avoid over-discharge or overcharge conditions that will reduce the cycle life of the battery.
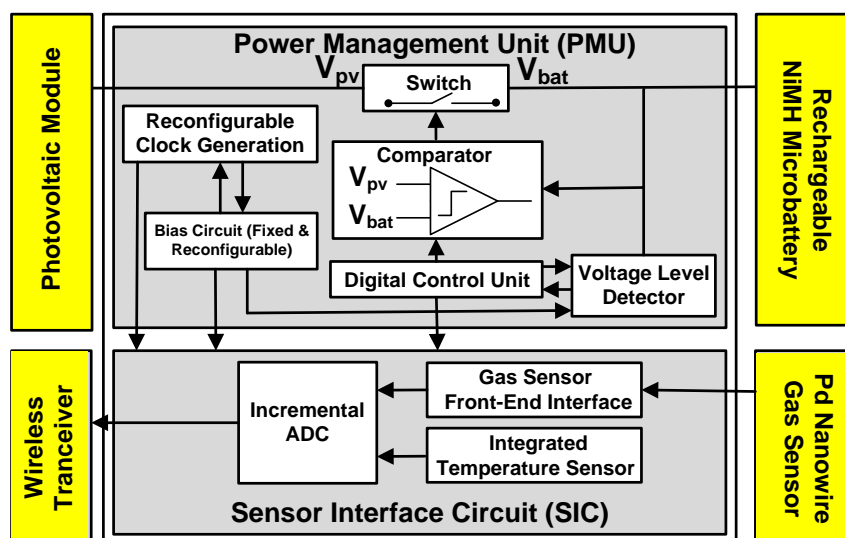
Figure 1. Block diagram of the SiNAPS electronic circuit.

For the PV solar cell, nanowires are prepared by metal assisted wet chemical etching on an n-type silicon wafer [32]. This method produces random arrangements of nanowires with diameters in the 20 nm to 200 nm range. The length of the nanowires is determined by the etching time. For etching we use a solution of HF/AgNO3. When AgNO3 gets into contact with the silicon, silver nanoparticles form which act as catalysts for the silicon etching. Only at positions where these particles are located etching occurs so that at the particle free regions nanowires remain. After etching the silver particles have to be removed carefully. Around the nanowires amorphous hydrogenated silicon is deposited by conventional PECVD. First an about 1 nm thin intrinsic layer is deposited followed by about 10 nm of p-type a-Si:H forming the p-n junction as in Sanyo's HIT (heterojunction with thin intrinsic layer) concept [33]. For passivation this active structure is covered by an about 1 nm thin Al2O3 layer, deposited by atomic layer deposition (ALD). For contacting the structure, the space between the nanowires is filled with a transparent conductive oxide. We use aluminum doped ZnO deposited by ALD [11]. The complete solar cell structure is shown in the TEM cross section of Figure 2.
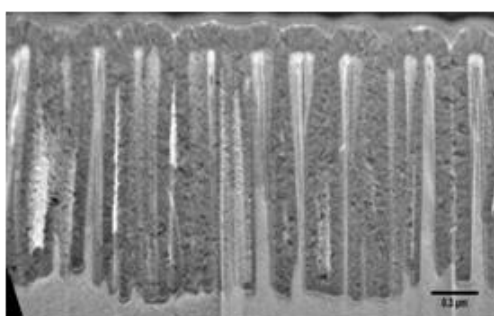

Figure 2. TEM cross section of nanowire solar cell. The nanowires are single crystalline and n-type with the p-n junction in core shell configuration by covering the nanowires with a shell of p-type amorphous silicon.

For preparation of the SiNW sensor an SOI wafer with p-doped top Si layer of 70 nm, buried oxide (BOX) SiO_2 layer of 145 nm, and base silicon layer of 500 μm (Soitec) is used in this study. The top device layer of the SOI wafer was oxidized to form a thin SiO_2 of 45 nm via dry thermal oxidation. As a result, the thickness of the device layer was reduced from 70 nm to 44 nm. Then it was doped with boron (B) by ion implantation to a dose of 4×10^{13} cm^{-2} at ion energy of 14k eV and a tilt angle of 7°. The dopant activation was done by furnace annealing at 900 C for 30 min in

nitrogen environment. The effective doping concentration in the Si device layer was measured to be equivalent to ~1 × 10^{18} cm^{-3}.

Afterward, two EBL exposures were done on a full 4" SOI wafer with JEOL JBX 6000FS Gaussian beam direct write system operated at 50 kV. In the first exposure, the alignment marks were defined in a 425 nm thick layer of ZEP520A positive resist (Nippon ZEON Corp.) using the low-resolution high-current mode of the system. The marks were etched 1.5 μm deep through the ZEP mask with a two-stage plasma etching process. Then the resist was removed and the top SiO$_2$ layer wet etched in 10:1 buffered oxide etchant (BOE), resulting in Si device layer thickness of 44 nm. In the second EBL exposure, the nanowire devices (nanowires together with the source and drain contact pads) were defined in a 50 nm thick layer of hydrogen silsesquioxane (HSQ) negative tone resist (XR-1541 from Dow Corning Corp.) using the high-resolution mode of the system and a beam current of 100 pA. In order to ensure definition of resist structures down to 10 nm as well as full CMOS compatibility of the fabrication, an original high-contrast and low roughness development process with 25% tetramethylammonium hydroxide (TMAH) as a main step was implemented [34,35].

To transfer the HSQ lithographic pattern into the top Si layer, RIE process with chlorine (Cl) chemistry in a Plasmalab System 100 from Oxford Instruments was used. Subsequently, an additional 200 nm SiO$_2$ layer was deposited on the whole surface, except the device regions, to minimize the leakage current through the buried oxide. Next, the metal contacts and interconnection were created by deposition of 50 nm titanium (Ti) and 500 nm aluminium (Al) layers. Then, a passivation layer of 500 nm SiO$_2$ was deposited again on the whole surface, except the device regions and metal pads. These three subsequent depositions were done by electron beam evaporation in a Temescal FC-2000 system and were respectively combined with three steps of photolithography and lift-off. The photolithography exposures were aligned to the previously exposed EBL pattern using the etched alignment marks, i.e. a mix-and-match lithography was done. To improve the conductivity of devices, they were thermally annealed for 30 min at 425 °C in forming gas (10% H$_2$ / 90 % N$_2$). A cross-section of fabricated devices is schematically presented in Figure 3. Electrical measurements of devices as well as the ionic strength sensing experiments were done using cascade manual probe station and Agilent semiconductor analyser B1500.
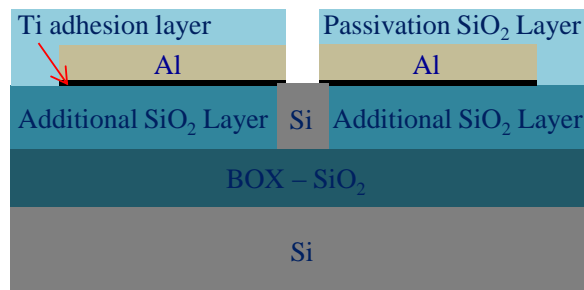

Figure 3.Schematic representation of the sensing device in cross section.

For fluid delivery, 200 μm-wide microchannels were fabricated in PDMS using standard protocol [36]. The PDMS stamps were bonded to the devices using the "stamp and stick" method [37]. A thin layer of uncured liquid PDMS was spread on a microscope slide onto which the PDMS stamp was placed. The stamp is then placed in position on the device using a micrometer-controlled positioning rig constructed in-house and subsequently bonded by curing the liquid PDMS in an oven at 60°C for ~1hr. To allow fluid access to the microchannel, 400 μm access holes were drilled into the PDMS stamp into which400 μm outer diameter polytetrafluoroethylene (PTFE) tubing was inserted. Fluid was delivered through the PTFE tubing and into the microchannels from gastight syringes (Hamilton) which were propelled by a syringe pump (Harvard Pump 11+) at a flow rate of 150 μL/min.

3. RESULTS AND DISCUSSION

3.1 Si Nanowire Solar Cells

Our solar cells prepared in this way reached an open circuit voltage of 517 mV, a short circuit current of 26.5 mA/cm², and an efficiency of 10.0% [10,11]. These results position the SiNAPS core-shell nanowire solar cells at the leading edge of this technology. An I-V curve of this solar cell is shown in Figure 4. For further reducing the volume of the device we are developing the nanowire solar cells on SOI wafers and on crystalline silicon thin films with a thickness of less than 10 µm. Our nanowire solar cells on 8 µm thin laser crystallized silicon films reached an efficiency of 8.8%.
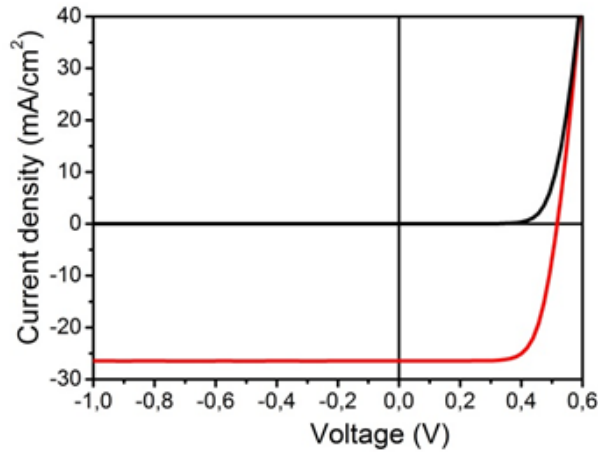

Figure 4. I-V curve of a core-shell Si nanowire solar cell.

For powering the sensor electronics and the battery, a voltage of at least 1.2 V is required, Sec. 2. Therefore to ensure that the necessary voltage is delivered from the PV, 4 solar cells of this type have to be connected in series to form a minimodule. To deliver the required power of 40 µW, a total solar cell area of 1.6 mm² is needed with a single solar cell of dimensions 0.5x0.8 mm². For the series connection of the cells we use wire bonding as sketched in Figure 5. A simple test module consisting of eight such solar cells is shown in Figure 6. Figure 6 also shows the I-V curves under AM1.5 illumination. The curves refer to a single cell (black dots), two cells connected in series (red dots), three cells (green dots), and so on. The right most curve applies to the complete module. As it can be deduced from these data, the module delivers an open circuit voltage of 2.4V. The maximum output power is about 190 µW at V_{MPP} of 1.83 V.
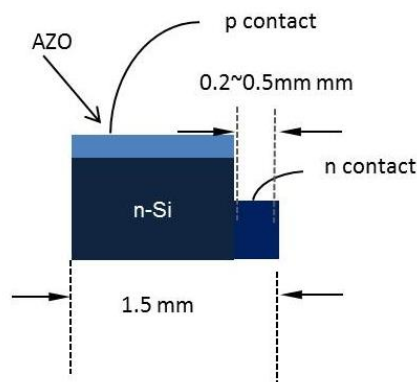

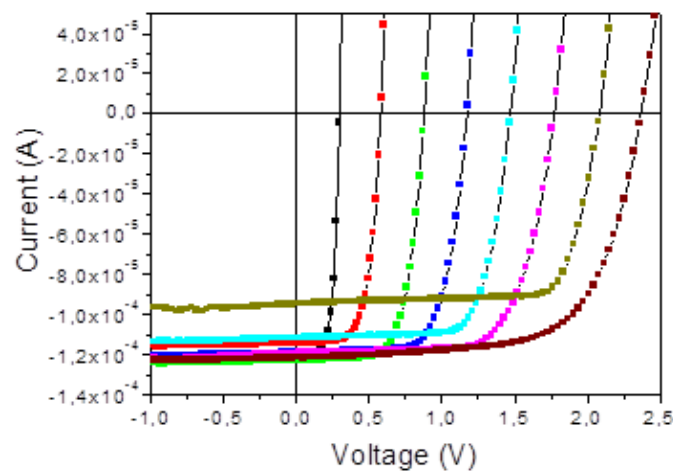Figure 5. Contacting scheme of nanowire solar cell to form a PV minimodule.

Figure 6. Simple minimodule with a total area of 7.8 mm² consisting of 8 nanowire solar cells connected in series by wire bonding (top) and I-V curves under AM1.5 illumination of cells 1 to 8 of the module connected in series.

3.2 Microfluidic Delivery and Si NW Sensor

Using the top-down fabrication approach detailed above, a range of SiNW geometries can be generated. 45 different geometries were fabricated: three sets, each with a different number of nanowires (1, 3, and 20 SiNW) and lengths (0.5, 1, and 10 µm) of channel nanowires (NWs) as well as five different NW widths (10, 20, 30, 50 and 5000 nm). Figure 7(A) shows an example of scanning electron microscopy (SEM) images of SiNW junctions consisting of 1,3,and 20 nanowires of 20 nm width and 1000 nm length. The structures exhibited minimal roughness (between 0.8 and 1.6 nm) and negligible deviation from the prescribed widths. I_d-V_d plots showed the devices to have good ohmic contacts (data not shown) whilst I_d-V_{bg} plots (Figure 7(B)) showed the devices could operate well as backgated junctionless transistors.The electrical characterisation of the SiNWs shows them to be promising candidate for sensing applications.

SiNW-based devices have previously been used to sense individual biomolecule binding events [20,38], as well as more general fluid properties such as pH [20,25]. Regardless of the sensing operation being performed, there is a requirement that analyte can be delivered to the sensing structures whilst being contained away from the rest of the device. Hence the SiNW sensor devices were integrated with microfluidic channels fabricated in polydimethylsiloxane (PDMS) to create an integrated sensor/fluid delivery device, as described in the Experimental section. Example images of the resulting integrated devices are shown in Figure 8.
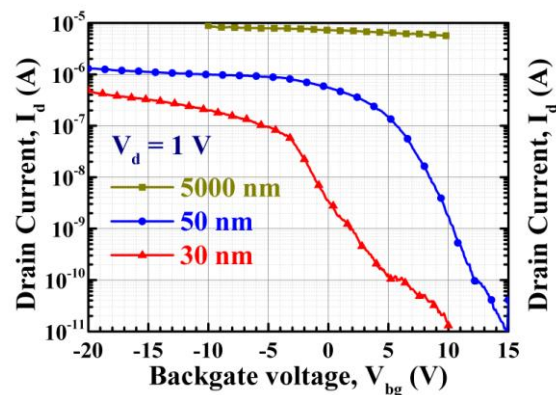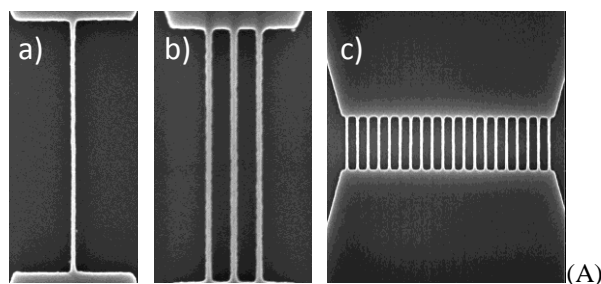
Figure 7.(A) SEM images of devices composed of a) 1, b) 3 and c) 20 Si NWs. In each case the wires are 1 μm long and 20 nm wide. (B) I_d-V_{bg} curves of devices composed of single SiNWs of length 1 μm and widths of 30, 50, and 5000 nm.

For practical applications such as in-the-field diagnostics, the most useful form of fluid delivery is *via* passive capillary action- obviating the need for any exterior pumping equipment to propel the analyte through the device. Passive delivery can be can be achieved in PDMS devices by careful design of the channel geometry and, most importantly, by rendering the channel surface hydrophilic using a suitable functionalization protocol [39]. For the exploratory testing carried out here, however, hydrodynamic delivery of the analyte from a syringe pump via PTFE tubing was deemed more appropriate-offering the ability to easily and repeatedly fill and empty the channel with different solutions as required.
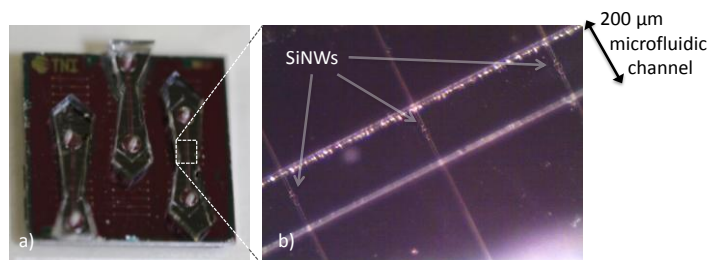

Figure 8. a) Image of the integrated device. Three microfluidic channels are shown attached to the chip-based sensor architecture. b) Microscopic image showing the microfluidic channel positioned above three separate SiNW sensor junctions.

As a proof-of-concept demonstration of the sensing capability of the integrated device, its capacity to sense solutions of different ionic strength was tested. For these experiments, a commercially available pH7 buffer was diluted using de-ionised water to generate a series of solutions of different ionic strength with equivalent pH. These were delivered to the NW sensors through the microfluidic channel. Figure 9 shows how the drain current changed over time as the solutions were administered. The current showed a clear and reproducible dependence on the relative concentration of the buffer

and hence the ionic strength of the solution, with increased ionic strength leading to increased drain current. Furthermore, the repeated measurement of the most concentrated solution shows the measurements to be reproducible.
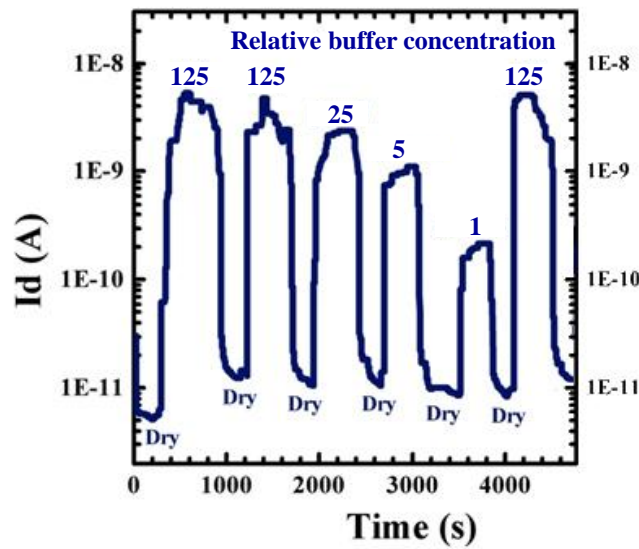

Figure 9.Time dependence of the drain current Id whilst pH7 buffer solutions of various concentration are flown through the channel. Air was used to dry the channel in between administrations of buffer.

3.3 Energy Harvesting and Power Management

The proposed energy harvester is based on the direct charging scheme, in which the battery is connected to the PV module using a PMOS switch. A dynamic comparator compares battery and PV voltages, V_{bat} with V_{pv}, to avoid discharge of the battery when V_{pv} is less than V_{bat} (see Figure 1). When the PV module is small and can only provide a few micro-watts under reduced light intensity, only low-overhead schemes that incur very little power overhead can be good candidates. In direct charging, as V_{pv} always follows V_{bat}, only the design time component matching (DTCM) approach can be used for maximum power point tracking [40]. In order to achieve high efficiency, the maximum power point voltage (V_{mpp}) of the PV module should be close to the V_{EOC} of the battery. Although P_{mpp} and I_{SC} of the PV module can change under lightning conditions, V_{oc} and V_{mpp} of the PV module do not change significantly [30]. When the target NiMH microbattery is discharged by a low current V_{bat} remains almost constant, up to getting close to the fully discharged state. However, when the battery is discharged by a high current, V_{bat} drops immediately and the voltage drop depends on the remaining charge of the battery [27].

During wireless data transmission, the battery is discharged by a high current, close to 5 CA (C being the 1 hour charge or discharge current) and by detecting the battery voltage during this period, the energy stored in the battery can be estimated accurately. A switched-capacitor voltage level detector (LD) block detects the battery voltage level starting from V_{EOD} of 0.9 V up to V_{EOC} of 1.5 V. After measuring V_{bat} and estimating the energy stored in the battery, the power management circuit reconfigures power-performance of the microsystem to guarantee autonomous sensor operation. If V_{bat} is sufficient, power management and sensor interface circuits work at their highest speed, and measurement results are sent to the base station every 15 seconds. If V_{bat} is not high enough, these blocks are activated with a lower duty cycle to minimize average power consumption. The power consumption and speed of digital circuits are reduced by reconfiguring the frequency in the used current-starved oscillator [41]. At the same time, in ultra-low power analog circuits, such as the discrete time incremental ADC that has been used for sensor interfacing, bias currents should be high enough to guarantee correct operation at the target clock frequency. When reducing the clock frequency the bias currents in the sensor interface circuit are scaled down dynamically to further reduce the power consumption of analog circuits. A switched-capacitor beta-multiplier (SCBM) current source that generates frequency-proportional bias currents is used for this purpose [41]. In addition, a fixed 10 nA beta-multiplier (BM) current reference provides the required bias currents for clock generation and LD blocks. The digital control unit (DCU) activates the comparator and LD blocks. As

neither V_{bat} nor V_{pv} change rapidly, these blocks are activated every few seconds and DCU generates the required control signals for related SC circuits.

Table 1 presents die area and power consumption of individual blocks, operating at 1 MHz clock frequency. The PV module, with the total area of $4mm^2$, can provide a maximum power of 319.5µW at V_{mpp} under AM1.5 illumination level The average power consumption of the sensor interface circuit depends on sampling rate. By measuring H_2 concentration and temperature in every 100ms, average power consumption will be *ca.* 140 nW. The simulated total power consumption of the circuit is primarily determined by the always active clock generator, bias circuit and DCU blocks. The power consumption of DCU is mainly determined by the low frequency 20-bits counter that activates the comparator and LD. Although comparator and LD blocks consume considerable power during their active time, nevertheless, as they are activated every 10 seconds, their average power consumption is less than 1 nW. When V_{bat} is low, the average power consumption of the sensor interface circuit, clock generator and DCU blocks is reduced by operating at a lower frequency [30]. The circuit has been implemented in 0.18µm CMOS process with $0.25mm^2$ total area as can be seen in the chip microphotograph in Figure 10. The main blocks including digital and analog blocks of solar energy harvester and sensor interface circuits have been specified separately. When operating at 1MHz, wireless transceiver sends the measurement results for both temperature and H_2 concentration to a base station every 15 seconds and the whole circuit consumes almost 2.1µW; while the average power consumption of the energy harvester is less than 350nW [30].

Table 1. Die area and active power of main blocks in the sensor

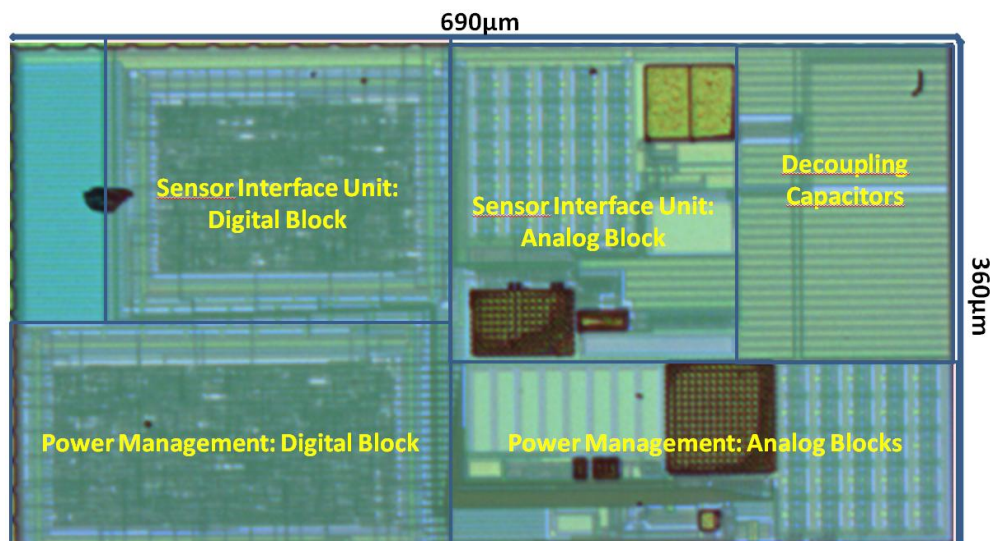| Block	Die Area (µm2)	Active Power (nW)	Average Power (nW)
Clock generator	14,400	165	165
Digital control unit	38,115	90	90
Bias circuit (10 nA)	2,832	35	35
Comparator	759	55	<1 nW
Level detector	31,960	520	<1 nW
SCBM	6,300	640	<1 nW
Sensor interface circuit	99000	1730	140

Figure 10. Chip microphotograph of the SiNAPS microsystem.

The power delivered to the battery by the PV module can be simulated using the equivalent circuit model of the PV module. In order to evaluate autonomous operation of the sensor, the power that can be delivered to the battery from PV module should be simulated in lower illumination levels. As can be seen in Figure 11, under simulated 10% of AM 1.5 illumination, 24.45µW power is delivered to the battery with 90.7% efficiency and the harvested energy is enough for autonomous operation of whole system. Meanwhile, as the whole sensor node consumes less than 16µA for sensing and data transmission, target 6mAh battery can provide enough power for approximately 375 hours operation, even without energy harvesting.
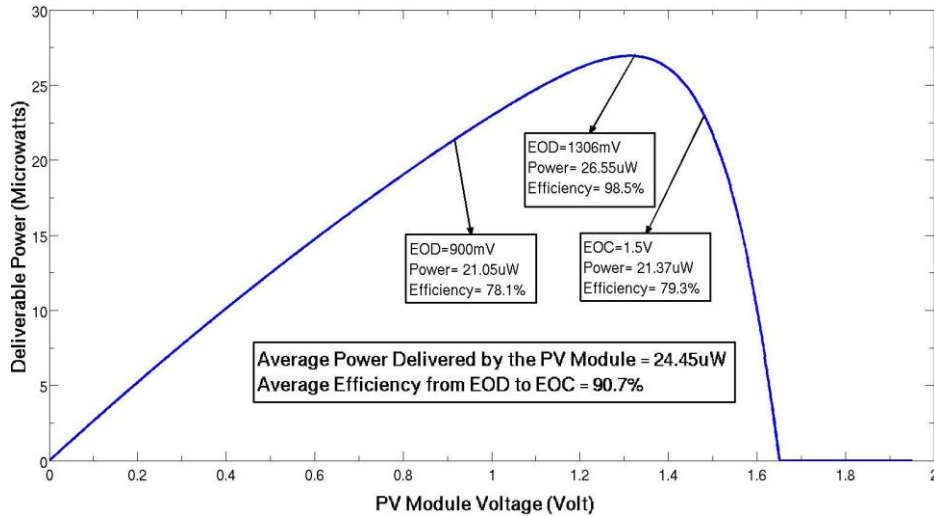

Figure 11. Power delivered to the battery under simulated 10% of AM1.5 illumination.

3.4 Low Power Sensor Interface Circuit

An application in gas sensing using a Pd nanowire grid with 14 Pd nanowires [6] will be used to test the proof-of-concept SiNAPS mote. Half of the nanowires are coated with a passivation layer to prevent hydrogen from reaching the nanowire, are only sensitive to temperature and are used as a reference. The remaining nanowires are sensitive to temperature and H_2 concentration, are used as sensors. The sensor interface circuit measures the conductance change of the sensing nanowires compared to to the reference nanowires. The measurement eliminates the first order temperature effect and is only sensitive to the ratio of conductance of nanowires, instead of their absolute values giving a higher accuracy.

The sensor interface circuit measures temperature and H_2 concentration and an incremental analog to digital converter (ADC) converts the measured analog values to 12-bit digital values [42]. Although by using sensing and reference nanowires the temperature effect is eliminated by the first order, as the temperature coefficient of Pd nanowire resistance changes according to H_2 concentration, there are still second order effects. In order to compensate this second order effect, temperature is measured and incorporated during sensor calibration to increase H_2 sensing accuracy using an integrated temperature sensor [43].The sensor interface circuit consumes 1.73µW at 1MHz and as ADC needs 2^N cycle for n-bits conversion, a 12-bit conversion takes nearly 4ms [30].

Four operation modes have been defined according to the remaining charge of the battery that is estimated accurately by detecting the battery voltage during wireless data transmission. If a lower battery voltage is detected and the system is switched to a lower clock frequency to decrease the average power consumption of the whole system. In S_{L3} mode, that the remaining charge of the battery is more than 80%, the system operates at 1 MHz frequency and the samples are sent every 15 seconds. The average current consumption of Pd nanowire sensors and wireless transmission are 4.67µA and 9.4µA respectively in this operation mode and the total average current consumption of the whole sensor is less than 16µA [30].In fact, Pd nanowires should be biased with a 7µA bias current for 10 seconds, before measuring H_2 concentration and TZ1053 consumes 5µA during standby and consumes 3.3mA during a period of 20ms to send a sample with the minimum payload size of 55 bytes [16]. In S_{L2} and S_{L1} modes, the operating frequency is decreased to 500 KHz and 250 KHz respectively. In S_{L0} mode that the remaining charge of the battery is less than 25%, the circuit consumes less than 0.6µW by operating at 125 KHz frequency instead of 1MHz and using lower bias currents. The

average power consumption of the energy harvester drops to less than 110nW in S_{L0} mode. In addition, measurement results are sent every 120 seconds instead of every 15 seconds in S_{L3} mode, to further reduce the total average power consumption of the whole sensor to less than 7μA.

4. CONCLUDING REMARKS

A materials technology platform based on nanowires have enabled us to develop and optimize miniaturized components (die area ~1mm^2) of an autonomous wireless chemical sensor, the SiNAPS mote. State-of-the-art energy power consumption of the total system was established, including the power management unit and the sensor interface circuit, and proof-of-principle micropower energy harvesting was demonstrated with high efficiency miniaturized PV modules. Using Telran TZ1053 radio to send one sample measurement of both temperature and H2 concentration every 15 seconds, the average and active power consumption for the SiNAPS mote are less than 350nW and 2.1 μW respectively. The fabricated core (crystalline Si)-shell (amorphous Si) nanowire solar cells yield photovoltaic response of single solar cells with efficiencies up to 10% under AM1.5 illumination and an open circuit voltage, V_{oc}, of 450-500mV. Direct charging of a rechargeable battery is the most efficient method that fits the small size constraint and the energy budget while resolving the issue of intermittent energy harvesting. Matching of the nominal voltage has been achieved by connecting nanowire-based solar cell in series via wire bonding. The end-to-end efficiencies are up to 90% under under AM1.5 illumination (80% under 100 times reduced intensity).

Nanowire-modified CMOS platform are used for low-power miniaturised (bio-)chemical sensors. Two sensor platforms have been developed, one for examining liquid analytes through microfluidic delivery to surface functionalised silicon nanowires and the other to sense hydrogen gas. Junctionless sensing devices based on Si nanowire structures of controllable geometry (width, length and number of nanowires) were fabricated with high precision by a top-down process on SOI wafers. The quality of the patterning was very high and resulted in structures with low roughness (between 0.8 and 1.6 nm) and minimum deviations of the SiNW widths from the designed ones. Their electrical characterisation shows the devices perform well as backgated junctionless transistors. The SiNW sensing devices have been successfully combined with microfluidic channels fabricated in PDMS to form an integrated device which allows delivery and subsequent sensing of liquid samples. As a proof-of-concept, the integrated device was shown to be able to sense the relative concentration of a pH7 buffer solution. The hydrogen sensor platform is based on palladium nanowires and its principle has been discussed elsewhere. Here, details were given of the sensor interface circuit that presents the additional challenge of temperature compensation since the resistivity of Pd nanowires is sensitive to temperature. We estimate that hydrogen gas concentrations can be detected in the 100-100,000 ppm range and a broad temperature range. This work and our current effort in the sensor system integration will provide the basis for a paradigm shift in the miniaturization of sensor nodes and their wider application in (bio-)chemical monitoring, enabled by the nanowire materials platform.

REFERENCES

[1] Vullers, R. J. M., Schaijk, R. V., Visser, H. J., Penders, J., Hoof, C. V., "Energy harvesting for autonomous wireless sensor networks", IEEE Solid-St. Circ. Mag., 2, 29-38, (2010).

[2] ÓMathúna, C. ,O'Donnell, T, Martinez-Catala, R. F. , Rohan, J., O'Flynn, B., "Energy scavenging for long-term deployable wireless sensor networks", Talanta, 75, 613–623, (2008).

[3] Barton, J., Harte, Jung, E., "Distributed, embedded sensor and actuator platforms", in [Augmented Materials and Smart Objects: Building Ambient Intelligence Through Microsystems Technology], Springer Science + Business Media, New York, 105-129, (2008)

[4] Penders, J., Gyselinckx, B., Vullers, R., De Nil, M., Nimmala, S., Van de Molengraft, J., Yazicioglu, R., Torfs, T., Leonov, V., Merken, P., Van Hoof, C., "Human++: From technology to emerging health monitoring concepts", Proc. 5th Int. Workshop Wearable and Implantable Body Sensor Networks, 94–98 (2008).

[5] Semiconducting Nanowire Platform for Autonomous Sensor, <www.sinaps-fet.eu> (29 March 2013).

[6] Van der Bent, J. F., Van Rijn, C. J. M., "Ultra low power temperature compensation method for palladium nanowire grid", Procedia Engineering, 5, 184-187 (2010).

[7] Cook, B. W., Lanzisera, S. Pister, K. S. L., "SoC Issues for RF smart dust", Proc. IEEE 94, 1177-1196 (2006).

[8] Conibeer, G., "Third-generation photovoltaics", Materials Today, 10, 42- 50 (2007).

[9] Peng, K.-Q., Lee, S.-T, "Silicon nanowires for photovoltaic solar energy conversion", Adv. Mat., 23, 198-215 (2011)

[10] Jia, G., Eisenhawer, B., Dellith, J., Falk, F., Thøgersen, A. and Ulyashin, A., "Multiple core-shell silicon nanowire-based heterojunction solar cells", J. Phys. Chem. C 117, 1091-1096 (2013).

[11] Steglich, M., Bingel, A., Jia, G., Falk, F., "Atomic layer deposited ZnO:Al for nanostructured silicon heterojunction solar cells", Sol. Energ. Mat. Sol. Cells., 103, 62-68 (2012).

[12] Song, T., Lee, S.-T., Sun, B., "Silicon nanowires for photovoltaic applications: The progress and challenge", Nano Energy, 1, 654–673 (2012)

[13] Green, M. A., Emery, K., Hishikawa, Y. Warta, W., Dunlop, E. D., "Solar cell efficiency tables", Prog. Photov. Res. App., 20, 606-614 (2012).

[14] Datasheet Imote 2, "High-performance Wireless Sensor Network Node", 2009, <www.xbow.com> (25 December 2012)

[15] Gislason, D., [ZigBee Wireless Networking], Newnes Publications, London, (2008).

[16] Qiu, Y., Liempd, C.V., Veld, B.O.H., Blanken, P.G., Hoof, C.V., "5μW-to-10mW input power range inductive boost converter for indoor photovoltaic energy harvesting with integrated maximum power point tracking algorithm", Proc. IEEE International Solid-State Circuits Conference, San Francisco, USA, 118–120, (2011).

[17] Chen, G., Ghaed, H., Haque, R., Wieckowski, M., Yejoong K., Gyouho K., Fick, D., Daeyeon K., Mingoo S., Wise, K., Blaauw, D., Sylvester, D., "A cubic-millimeter energy-autonomous wireless intraocular pressure monitor", Proc. IEEE International Solid-State Circuits Conference, San Francisco, CA, USA, 310-312, (2011).

[18] Fasoli, A., Milne, W. I., "Overview and status of bottom-up silicon nanowire electronics", Mat. Sci. Sem. Proc., 15, 601–614 (2012).

[19] Cui, Y. Lieber, C. M., "Functional nanoscale electronic devices assembled using silicon nanowire building blocks", Science, 291, 851-853 (2001).

[20] Cui, Y., et al., "Nanowire nanosensors for highly sensitive and selective detection of biological and chemical species", Science, 293, 1289-1292 (2001).

[21] Patolsky, F., Zheng, G., Lieber, C. M., "Fabrication of silicon nanowire devices for ultrasensitive, label-free, real-time detection of biological and chemical species", Nat. Protocols, 1, 1711-1724 (2006).

[22] Buitrago, E., Fagas, G., Fernández-Bolaños Badia, M., Georgiev, Y. M., Berthomé, M., Ionescu, A. M., "Junctionless Silicon Nanowire Transistors for the Tunable Operation of a Highly Sensitive, Low Power Sensor", Sens. Act. B, *in press* (2013).

[23] Nair, P. R., Alam, M. A., "Design considerations of silicon nanowire biosensors", IEEE Trans. Elec. Dev., 54, 3400-3408 (2007).

[24] Park, I., et al., "Towards the silicon nanowire-based sensor for intracellular biochemical detection", Bios. Bioel., 22, 2065-2070 (2007).

[25] Park, I., et al., "Top-down fabricated silicon nanowire sensors for real-time chemical detection", Nanotechnology, 21, 015501 (2010).

[26] Jakeway, S. C., de Mello, A. J., Russell, E. L., "Miniaturized total analysis systems for biological analysis" Fresenius J. Anal. Chem., 366, 525-539 (2000).

[27] Varta V6HR Datasheet, <http://www.varta-microbattery.com> (25 March 2013).

[28] Toumaz TZ1053 Datasheet, <http://www.toumaz.com/page.php?page=telran> (25 December 2012).

[29] Zarlink ZL70250 Datasheet, <http://www.zarlink.com/zarlink> (25 December 2012).

[30] Khosro Pour, N., Krummenacher, F., Kayal, M., "Fully Integrated Solar Energy Harvester and Sensor Interface Circuits for Energy-Efficient Wireless Sensing Applications", J. Low Power Electron. Appl., 3, 9-26. (2013).

[31] Khosro Pour, N., Krummenacher, F., Kayal, M., "Fully integrated ultra-low power management system for micro-power solar energy harvesting applications", Elec. Lett., 48, 338-339 (2012).

[32] Peng, K. Q., Yan, Y. J., Gao, S.-P., Zhu, J., "Synthesis of large-area silicon nanowire arrays via self-assembling nanoelectrochemistry", Adv. Mater.14, 1164-1167 (2002).

[33] Mishima, T., Taguchi, M., Sakata, H., Maruyama, E., "Development status of high-efficiency HIT solar cells", Sol. Energ. Mat. Sol. Cells., 95, 18-21 (2011).

[34] Georgiev, Y.M., et al., "Surface roughness of hydrogen silsesquioxane as a negative tone electron beam resist", Vacuum, 77, 117-123 (2005).

[35] Henschel, W., Georgiev, Y. M., Kurz, H., "Study of a high contrast process for hydrogen silsesquioxane as a negative tone electron beam resist", J. Vac. Sci. Techol. B, 21, 2018-2025 (2003).

[36] Duffy, D. C., et al., "Rapid Prototyping of Microfluidic Systems in Poly(dimethylsiloxane)", Anal. Chem., 70, 4974-4984 (1998).

[37] Satyanarayana, S., Karnik, R. N., Majumdar, A., "Stamp-and-stick room-temperature bonding technique for microdevices", J. Microelectromech. Syst., 14, 392-399 (2005).

[38] Lin, T.-W., et al., "Label-free detection of protein-protein interactions using a calmodulin-modified nanowire transistor", PNAS, 107, 1047-1052 (2010).

[39] Demming, S., et al., "Characterization of long-term stability of hydrophilized PEG-grafted PDMS within different media for biotechnological and pharmaceutical applications", Phys. Stat. Sol. (a), 208, 1301-1307 (2011).

[40] Lu, C., Raghunathan, V., Roy, K., "Maximum power point considerations in micro-scale solar energy harvesting systems", Proc. IEEE International Symposium on Circuits and Systems (ISCAS), Paris, France, 273–276 (2010).

[41] Pastre, M., Krummenacher, F., Kazanc, O., Khosro Pour, N., Pace, C., Rigert, S., Kayal, M., "A solar battery charger with maximum power point tracking", Proc. 18th IEEE International Conference on Electronics, Circuits and Systems (ICECS), 394-397, (2011).

[42] Markus, J., Silva, J., Temes, G. C., "Theory and applications of incremental $\Delta\Sigma$ converters", IEEE Trans. Circ. Syst. I, 51, 678- 690 (2004).

[43] Pertijs, M. A. P., Makinwa, K. A. A., Huijsing J. H., "A CMOS smart temperature sensor with a 3σ inaccuracy of $\pm0.1°C$ from -55°C to 125°C", IEEE J. Solid-St. Circ., 40, 2805- 2815 (2005).